THE JOURNAL OF PHYSICAL CHEMISTRY Letters

Letter

pubs.acs.org/JPCL

Photochemical Charge Separation in Nanocrystal Photocatalyst Films: Insights from Surface Photovoltage Spectroscopy

Jing Zhao and Frank E. Osterloh*

Department of Chemistry, University of California, Davis, One Shields Avenue, Davis, California 95616, United States

ABSTRACT: Photochemical charge generation, separation, and transport at nanocrystal interfaces are central to photoelectrochemical water splitting, a pathway to hydrogen from solar energy. Here, we use surface photovoltage spectroscopy to probe these processes in nanocrystal films of $HCa_2Nb_3O_{10}$, a proven photocatalyst. Charge injection from the nanoparticles into the gold support can be observed, as well as oxidation and reduction of methanol and oxygen adsorbates on the nanosheet films. The measured photovoltage depends on the illumination intensity and substrate material, and it varies with illumination time and with film thickness. The proposed model predicts that the photovoltage is limited by the built-in potential of the nanosheet−metal junction, that is, the difference of Fermi energies in the two materials. The ability to measure and understand these light-induced charge separation processes in easy-to-fabricate films will promote the development of nanocrystal applications in photoelectrochemical cells, photovoltaics, and photocatalysts.

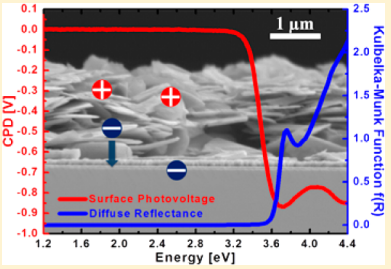

SECTION: Energy Conversion and Storage; Energy and Charge Transport

Photochemical charge separation on the nanoscale is of central importance for solar energy conversion with inorganic nanocrystals.[1] Analytical methods for this process rely mostly on the measurement of electrical currents[2−7] or optical changes.[8] Surface photovoltage spectroscopy (SPS) is a contactless technique that probes contact potential difference changes (ΔCPD) in thin films upon excitation with light.[9,10] The sensitivity of the method is higher than that of photoelectrochemistry because even small charge carrier concentrations (10^{10} per cm^2) yield potentials on the mV scale. Historically, SPS has been applied to the characterization of bulk semiconductors and surfaces, but in recent years, the method gained popularity for the study of integrated devices and microheterogeneous systems, notably by Thomas Dittrich's group.[11−16] In our research, SPS has been used to characterize nanoscale photocatalysts for water splitting reactions[17,18] and recently also for organic polymers employed in photovoltaics and organic light-emitting devices.[19] In these systems, the origin of the photovoltage is not always easy to elucidate. It can arise from the reorientation of permanent dipoles in the films, charge separation at the surface, inhomogeneous illumination (Dember effect),[20,21] and other processes. The identification of the mechanism then becomes central to the interpretation of the data. Here, we describe the results of a comprehensive SPS study on nanostructured crystalline films, where the light intensity, film thickness, substrates, and ambient were varied. Both intrinsic and surface states in the nanocrystals, redox reactions on the nanocrystal surface, and charge injection into the substrate can be resolved as a function of photon energy. The sign and size of the photovoltage signals can be quantitatively understood on the basis of a thermodynamic model for an illuminated semiconductor−metal junction. These results provide the basis for more systematic studies on photochemical charge transport and separation in nanocrystal films. They are relevant to the development of nanocrystal-based excitonic solar energy conversion systems.

Nanocrystal Films. Tetrabutylammonium-supported $TBA_xH_{(1-x)}Ca_2Nb_3O_{10}$ nanocrystals are known to promote a water splitting reaction upon band gap (3.5 eV) excitation.[22−24] These nanocrystals have a perovskite structure consisting of $Nb(\mu_2\text{-}O)_6$ octahedra with Ca^{2+} cations filling the voids (Figure 1A) and adopt a 2-D sheet-like morphology (Figure 1B). According to TEM images, nanosheets are ∼1.2 nm thick[25] but have lateral dimensions above 1 μm.

Thin films of the sheets on gold substrates were obtained by drop-coating from a dilute suspension, followed by drying at 100 °C for 10 min. The film thickness was varied from 57 to 6000 nm, depending on preparation conditions. In these films, nanosheets adopt a preferential coplanar orientation with regard to the substrate, as shown in Figure 1C/D. For SPS measurements, nanosheet films were placed in a vacuum chamber, and their changes in contact potential difference were measured as a function of photon energy.

Surface Photovoltage Spectra. A typical photovoltage spectrum has four distinct features I−IV (Figure 2A). Feature I is a negative ΔCPD signal at photon energies below the band gap of the material. This sub-band gap feature is attributed to the excitation of midgap defect states, likely at the surface of the nanosheets, and it becomes significant in the case of a poorly prepared sample, as shown in Figure 2B. The negative sign of the voltage indicates electron transfer toward the gold substrate. Feature II is the dominant negative ΔCPD signal in the spectrum, which is assigned to the photochemical charge

Received: January 21, 2014
Accepted: February 9, 2014
Published: February 9, 2014

   dx.doi.org/10.1021/jz500136h | J. Phys. Chem. Lett. 2014, 5, 782−786

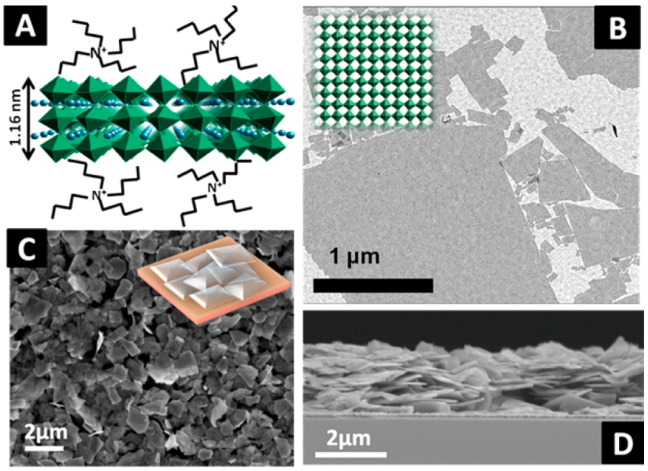

Figure 1. (A) Structural model and (B) TEM of $TBA_xH_{(1-x)}Ca_2Nb_3O_{10}$ nanosheets. (C) Top and (D) side SEM view of a nanosheet film on a gold substrate.

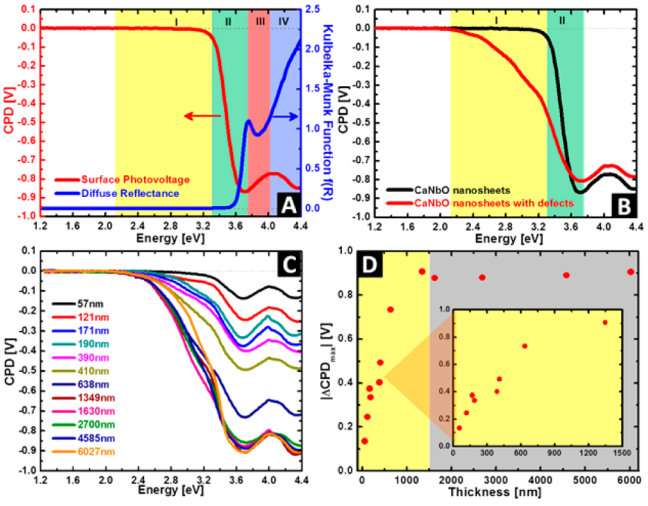

Figure 2. (A) Surface photovoltage spectrum of a $TBA_xH_{(1-x)}Ca_2Nb_3O_{10}$ nanosheet film on Au, along with its diffuse reflectance spectrum. (B) Photovoltage spectral comparison between low-defect and rich-defect samples. (C) Spectra of $TBA_xH_{(1-x)}Ca_2Nb_3O_{10}$ nanosheet films with a set of various thicknesses. (D) Peak photovoltage (ΔCPD_{max}) at 3.75 eV (330 nm) from (C) plotted as a function of film thickness.

separation under direct band gap excitation of $TBA_xH_{(1-x)}Ca_2Nb_3O_{10}$. This assignment is supported by the overlap of feature II with the optical absorption of the nanosheets (green region in Figure 2A). Features III and IV are also due to separation of charge carriers generated under band gap excitation. The dip of the signal at 3.8 to 4.0 eV is caused by the lower density of states (DOS) in this region, which is observed also in the optical absorbance spectrum. As suggested by DFT calculations on $KCa_2Nb_3O_{10}$, the high- and low-energy DOS can be assigned to the NbO_6 units at or away from the surface, respectively.[26]

As shown in Figure 2C, the main photovoltage features I/II (and to a lesser extent III/IV) depend on the film thickness. This dependence is plotted for feature (I+II) in Figure 2D. When the film thickness is below 1350 nm, the photovoltage increases linearly with film thickness, but above this value, the photovoltage remains constant. As will be discussed below, this behavior agrees with the metal−semiconductor junction model in Figure 4.

In order to study the dependence of features I/II on the light intensity, a nanosheet film was exposed to 3.75 eV (330 nm) illumination with various flux intensities. As shown in Figure 3A, both the size of the ΔCPD signal and its growth rate

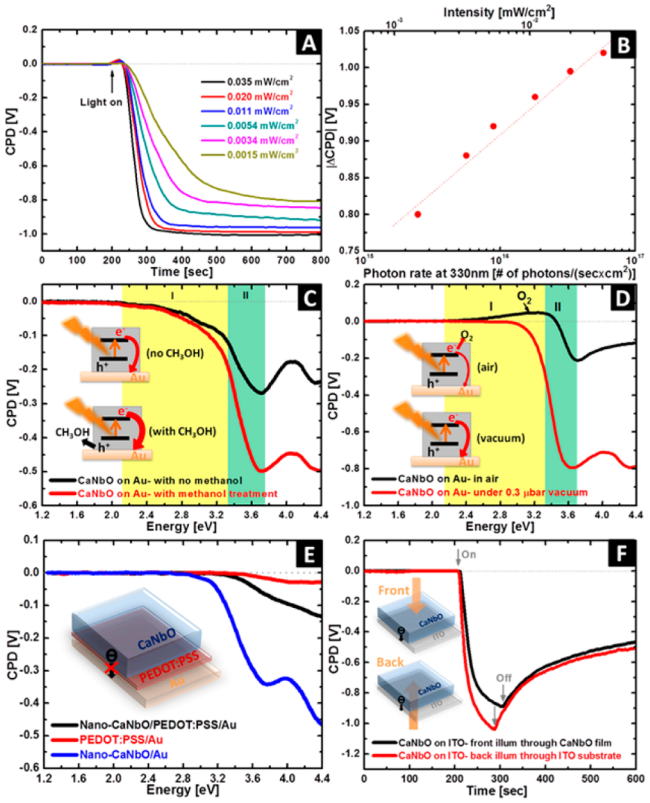

Figure 3. (A) Photovoltage responses of a nanosheet film (thickness > 1400 nm) under monochromatic illumination with a variable intensity (0.0015−0.035 mW/cm^2 at 330 nm, 3.75 eV). (B) Plot of ΔCPD versus the photon flux and power density from (A). (C) Photovoltage spectra of nanosheets in vacuum before versus after methanol treatment. (D) Photovoltage spectra of a nanosheet film in vacuum versus air. (E) Photovoltage spectra of nanosheets on a Au substrate with or without 40 nm poly(3,4-ethylenedioxythiophene) poly(styrenesulfonate) (PEDOT/PSS). (F) Comparison of time-dependent photovoltage signals for a thin film of a $TBA_xH_{(1-x)}Ca_2Nb_3O_{10}$ nanosheet on ITO between front-side and back-side illumination configurations under a ~25 mW/cm^2 Xe full spectrum.

increase with flux. A logarithmic plot of the steady-state signal versus the monochromatic flux (Figure 3B) is nearly linear. This is expected from the thermodynamics for an illuminated metal−semiconductor junction, as will be described below.

SPS was used also to detect the photochemical reactions of $TBA_xH_{(1-x)}Ca_2Nb_3O_{10}$ nanocrystals with methanol and oxygen. When a film was briefly exposed to drops of methanol before bringing it back into vacuum, the voltage at 3.75 eV nearly doubled (Figure 3C). This is attributed to the photochemical oxidation of surface-adsorbed methanol via photogenerated holes, which enables more electron transport to the gold substrate. On the other hand, when the spectrum was recorded in air (Figure 3D), feature II was greatly reduced, and a new positive signal appeared at 2.4−3.2 eV, which can be assigned to the photoreduction of oxygen from air. The low onset (2.4 eV) of this oxygen reduction signal suggests that midgap

dx.doi.org/10.1021/jz500136h | J. Phys. Chem. Lett. 2014, 5, 782−786

surface defects are involved in this electron transfer process. Reduction of oxygen[27] and oxidation of methanol[28] are important chemical processes at illuminated semiconductor surfaces. Similar redox reactions involving trap states likely also played a role in earlier SPS studies on CdSe and TiO_2.[29−31]

In order to determine the mechanism for charge separation in nanosheet films, spectra were recorded in the presence of a hole-selective, electron-blocking PEDOT/PSS interlayer between the nanosheet and the gold substrate (Figure 3E). It can be seen that this interlayer greatly diminishes the ΔCPD signal from the nanosheet film. This suggests that the photovoltage arises from electron transfer across the nanocrystal−gold interface or into states at the interface. The small residual photovoltage (−0.1 V at 3.5 eV) is assigned to the direct excitation of states at the nanosheet−PEDOT/PSS interface and PEDOT/PSS itself.

Previous photovoltage studies on C_{60} films have attributed charge separation to the Dember effect,[21] that is, to charge transport driven by carrier concentration gradients in *inhomogeneously* illuminated films.[20] In order to determine the presence of such a Dember photovoltage effect in the present system, a front versus back illumination experiment was conducted with a nanocrystal film exposed to the full spectrum of Xe illumination. As shown in Figure 3F, the photovoltage signal shows no significant change when the illumination direction is reversed. This suggests that the photovoltage does not arise from the Dember effect but from preferential electron transfer toward the gold substrate.

Mechanism of Charge Separation. The data in Figures 2 and 3 supports the semiconductor−metal junction model proposed in Figure 4. Due to their large band gap and low doping level, $TBA_xH_{(1-x)}Ca_2Nb_3O_{10}$ nanosheets do not contain a sufficient concentration of free charge carriers to achieve an electrochemical equilibrium with the gold substrate in the dark (Figure 4A). The loose packing of the nanocrystals also does not promote charge transfer. As a result, the nanosheet film on a gold substrate stays electrically neutral, and the initial CPD signal measured by the Kelvin probe is due only to the difference between work functions of the Kelvin probe and the metal support, including dipoles (e.g., water molecules) at the back interface. This situation changes under defect or band gap excitation, which generates charge carriers in the nanocrystal film. Of these carriers, the more mobile photoelectrons can inject into the gold support, while the photoholes accumulate on the nanocrystals in the film. The associated positive charging shifts the electric film potential to more positive values, which results in the observed contact potential change ΔCPD. In principle, a steady state is reached when the quasi-Fermi level $E_{F,n}$ in the illuminated nanosheet film and the Fermi level E_F of the gold support become equal. For a sufficiently thick film (>1350 nm) under 3.75 eV illumination (0.035 mW/cm^2), the maximum signal is measured as ΔCPD = −1.025 V (Figure 3B). Theoretically, for $TBA_xH_{(1-x)}Ca_2Nb_3O_{10}$ nanosheets at pH = 7, the built-in potential at the back interface is larger, $E_F(Au) - E_{F,n}(TBA_xH_{1-x}Ca_2Nb_3O_{10})$ = −5.3 eV[32] − (−3.5 eV)[22] = −1.8 eV. The lower experimental value of −1.025 V is probably due to the fact that electron transfer from the nanocrystals to the gold is accompanied by the competing hole transfer. The voltage is further limited by the finite illumination intensity and by the effects of permanent dipoles at the nanosheet−gold interface (Figure 4).[9,33] As shown in Figure 2C/D, the experimental ΔCPD values also strongly depend on the film thickness. This can be attributed to the charge

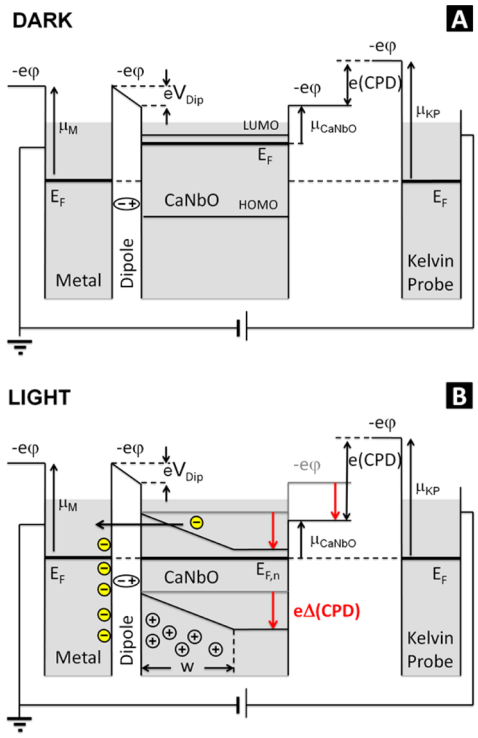

Figure 4. Energy diagrams for the metal−nanosheet−vacuum−Kelvin probe configuration in the dark (A) and under band gap illumination (B). Symbols: e: electron charge, φ: electric potential; CPD: contact potential difference; ΔCPD: light-induced CPD change; w: space charge layer width; μ_i: chemical potential (work function) of $TBA_xH_{(1-x)}Ca_2Nb_3O_{10}$, metal substrate, or Kelvin probe; V_{Dip}: potential drop from the interfacial dipole; E_F: Fermi level (electrochemical potential) in the dark; $E_{F,n}$: quasi-Fermi level of electrons under illumination, n_e: electron concentration; N_{CB}: effective DOS in the conduction band.

screening effect. In thin films (<1350 nm), the negative charge that accumulates at the gold−nanosheet interface (Figure 4B) is not completely screened by the spread-out positive charge in the nanosheet film. This negative charge is then felt at the film surface and reduces the positive electric potential of the film. Because the photoholes in the film are not mobile (they have previously been shown to generate surface peroxides),[23] the positive potential increases almost *linearly* with film thickness within the space charge layer, as observed in Figure 2D. The thickness w of this space charge layer is defined by the total charge separated at the gold nanosheet film interface and by the hole concentration on the nanocrystals in the film. Theoretically, the photovoltage is also limited by the finite light penetration depth of the niobates, which reduces the effective light intensity at the bottom part of the film. However, no such shading effect is observed within the thickness regime studied here. The observed dependence of the ΔCPD signal on the photon flux (Figure 3A/B) follows the thermodynamics of metal−semiconductor junctions. According to eq 1 (for symbols, see the Figure 4 caption), $E_{F,n}$ depends on the logarithm of the steady-state electron concentration n_e in the niobate conduction band. Because n_e scales with the absorbed photon flux,[3,24] ΔCPD has a logarithmic dependence on the photon flux (Figure 3B). Deviations from this trend could be due to the competitive hole transfer to the gold substrate and the trapping of electrons at defects or residual oxygen in the film.[9,33]

dx.doi.org/10.1021/jz500136h | J. Phys. Chem. Lett. 2014, 5, 782−786

$$E_{F,n} = E_{CB} - kT \ln \frac{n_e}{N_{CB}} \quad (1)$$

As seen in Figure 3C/D, the presence of redox-active molecules (O_2, CH_3OH) in the nanosheet film has a significant effect on ΔCPD. These molecules react with the photogenerated charge and thus act as local electron or hole sinks and alter the charge separation. Although a quantitative analysis of these ΔCPD data might provide additional useful information about the thermodynamics of these reactions, this analysis is beyond the scope of this Letter. Suggested by the proposed model in Figure 4, charge separation is largely determined by the build-in potential at the nanosheet−metal back interface; therefore, the photovoltage ΔCPD value varies significantly with an interlayer of PEDOT/PSS but remains when the illumination direction is reversed, as observed in Figure 3E/F.

In summary, we have demonstrated that SPS resolves charge transfer processes at solid−solid and solid−adsorbate interfaces in nanocrystal films, as a function of excitation energy. Variations in the DOS of the nanocrystals can be clearly observed, as well as effects resulting from surface defects, molecular adsorbates, and interfacial electron transfer barriers. Analysis of thickness-, substrate-, and intensity-dependent photovoltage data provides support for the metal−semiconductor junction model in Figure 4, which interprets the light-induced photovoltage as a result of the electrochemical equilibrium between the illuminated nanocrystals and the metal support. For sufficiently thick films (>w), the light-induced voltage can be used to evaluate the efficiency of photochemical charge separation at the sample−support interface, which in the ideal limit becomes equal to the built-in potential at the junction, that is, the difference of E_F(Au) and $E_{F,n}$(sample). The ability to apply SPS to evaluate photochemical charge separation in easy-to-fabricate nanocrystal films will aid nanocrystal applications in photoelectrochemical cells, photovoltaic devices, and photocatalysts.

EXPERIMENTAL METHODS

Chemical. Potassium carbonate (K_2CO_3), calcium carbonate ($CaCO_3$), niobium oxide (Nb_2O_5), and tetrabutylammonium hydroxide (TBAOH, 40 wt % aqueous solution) were obtained from Acros Organics, and HNO_3 (70%) was from Sigma−Aldrich. Chemicals were of reagent quality and used as received. PEDOT/PSS (Clevios P AI 4083) was used in the hole-conductive electron-blocking interlayer experiment. Au-coated (~80 nm) glass and ITO substrates (Resistance 4−8 Ω/sq, transmittance > 78%) were purchased from Thermo Scientific and Delta Technologies LTD, respectively, and cleaned before use. Pure water with a resistivity of >18 MΩ·cm from a Nanopure II water purifying system was used consistently through this study.

$TBA_xH_{(1-x)}Ca_2Nb_3O_{10}$ Synthesis and Film Preparation. $TBA_xH_{(1-x)}Ca_2Nb_3O_{10}$ nanosheets were synthesized according to a published procedure[23] and stored in an excess TBAOH aqueous solution at a pH > 10 to keep the nanosheets suspended without restacking. Before use, nanosheets were washed five times by centrifugation and resuspension in water to remove the excess TBA cations and bring the pH to neutral. The concentration of the nanosheets was determined by gravimetric analysis and diluted to 1 mg/mL for film preparation. Substrates of gold were cleaned by 30 wt % H_2O_2 aqueous solutions with 0.05 M KOH added and then rinsed with water thoroughly before use. ITO substrates were cleaned by a series of consecutive sonications in acetone, methanol, and isopropanol, followed by a final rinse with pure water. Unless stated otherwise, films of $TBA_xH_{(1-x)}Ca_2Nb_3O_{10}$ nanosheets were prepared by applying various volumes of 1 mg/mL nanosheet dispersion onto 1 × 1 cm^2 gold or ITO substrates and drying at 100 °C for 10 min. The resulting films have a thickness ranging between 50 nm and 6 μm, depending on the volume applied during film preparation. In the hole-conductive electron-blocking interlayer experiment, an interlayer of 40 nm PEDOT/PSS was spin-coated on a gold substrate before depositing $TBA_xH_{(1-x)}Ca_2Nb_3O_{10}$ nanosheets.

Characterization. Transmission electron microscopy (TEM) images of exfoliated $TBA_xH_{(1-x)}Ca_2Nb_3O_{10}$ nanosheets were taken with a Phillips CM-12 transmission electron microscope at an accelerating voltage of 120 kV. To prepare the TEM sample, $TBA_xH_{(1-x)}Ca_2Nb_3O_{10}$ nanosheets were washed and dispersed in water. Then, the particle dispersion was drop-casted onto a carbon-coated copper grid, followed by rinsing with water and air drying. Scanning electron microscopy (SEM) images of $TBA_xH_{(1-x)}Ca_2Nb_3O_{10}$ nanosheet films were obtained on a FEI XL30 high-resolution scanning electron microscope with an operating voltage at 5 kV. In the study of thickness dependence, film thickness was measured by a Veeco Dektak profilometer. UV−vis diffuse reflectance spectra of $TBA_xH_{(1-x)}Ca_2Nb_3O_{10}$ nanosheet films were recorded on a Thermo Scientific Evolution 220 UV−vis spectrometer equipped with an integrating sphere. The reflectance data were converted to the Kubelka−Munk function by $f(R) = (1 - R)^2/(2R)$ and plotted versus energy.

Surface Photovoltage Spectroscopy Measurements. Contact potential differences (CPDs) were recorded using a gold mesh Kelvin probe (3 mm diameter, Delta PHI Besocke) as the reference and controlled by a Kelvin control 07 (Delta PHI Besocke) with a sensitivity of 1 mV. Surface photovoltage spectroscopy (SPS) measurements were conducted using a 175 W Xe arc lamp (Atlas Specialty Lighting) as the light source, in conjunction with a monochromator (Cornerstone 130) to provide monochromatic illumination with an average peak FWHM of 15 nm. A typical photovoltage spectrum was recorded by monitoring CPD during a monochromatic scan from 1.2 to 5 eV (1000 to 250 nm). In the case of a time-dependent photovoltage measurement, a monochromatic illumination at 3.75 eV (330 nm) was applied. Meanwhile, the CPD signal was monitored over time to probe the photovoltage development upon illumination and decay when the illumination was off. In the case of a front versus back illumination experiment, the sample was deposited on an ITO substrate and placed in air outside of the vacuum chamber to enable the variation of the illumination configuration. Instead of a monochromatic illumination, a Xe full spectrum irradiation with an intensity of 25 mW/cm^2 on average was used in this case to enhance the photovoltage response in air. In all photovoltage measurements, the sample−probe distance was kept consistent (~1 mm) over various samples, and all measurements were performed under vacuum (10^{-7} bar) in a customized vacuum chamber powdered by a Pfeiffer HiCube 80 Eco turbo pump station, except for the front versus back illumination case, as specified above. Surface photovoltage results were corrected for signal drift due to the vacuum variation during the measurements by subtracting a linear drift background from the raw data, and all reported CPD values in Figure 2 and 3 are referenced against the dark CPD voltage.

dx.doi.org/10.1021/jz500136h | J. Phys. Chem. Lett. 2014, 5, 782−786

AUTHOR INFORMATION

Corresponding Author

*E-mail: fosterloh@ucdavis.edu.

Notes

The authors declare no competing financial interest.

ACKNOWLEDGMENTS

We are grateful for financial support from the Research Corporation for Science Advancement (Scialog award) and from the National Science Foundation (NSF, Grants 1152250 and 1133099). We thank Dr. Thomas Dittrich (Helmholtz Center Berlin) for insightful discussions.

REFERENCES

(1) Adams, D. M.; Brus, L.; Chidsey, C. E. D.; Creager, S.; Creutz, C.; Kagan, C. R.; Kamat, P. V.; Lieberman, M.; Lindsay, S.; Marcus, R. A.; et al. Charge Transfer on the Nanoscale: Current Status. *J. Phys. Chem. B* **2003**, *107*, 6668−6697.

(2) Bard, A. J. Photoelectrochemistry. *Science* **1980**, *207*, 139−144.

(3) Gerischer, H. Electrochemical Behavior of Semiconductors under Illumination. *J. Electrochem. Soc.* **1966**, *113*, 1174−1182.

(4) Krol, R. Photoelectrochemical Measurements. In *Photoelectrochemical Hydrogen Production*; van de Krol, R., Grätzel, M., Eds.; Springer: New York, 2012; Vol. *102*, pp 69−117.

(5) Bard, A. J.; Faulkner, L. R. *Electrochemical Methods: Fundamentals and Applications*, 2nd ed.; John Wiley: New York, 2001.

(6) Morrison, S. R. *Electrochemistry at Semiconductor and Oxidized Metal Electrodes*; Plenum Press: New York, 1980; Vol. *XIV*, p 401.

(7) Peter, L. M. Dynamic Aspects of Semiconductor Photoelectrochemistry. *Chem. Rev.* **1990**, *90*, 753−769.

(8) Subramanian, V.; Wolf, E. E.; Kamat, P. V. Catalysis with TiO_2/Gold Nanocomposites. Effect of Metal Particle Size on the Fermi Level Equilibration. *J. Am. Chem. Soc.* **2004**, *126*, 4943−4950.

(9) Kronik, L.; Shapira, Y. Surface Photovoltage Phenomena: Theory, Experiment, and Applications. *Surf. Sci. Rep.* **1999**, *37*, 1−206.

(10) Kronik, L.; Shapira, Y. Surface Photovoltage Spectroscopy of Semiconductor Structures: At the Crossroads of Physics, Chemistry and Electrical Engineering. *Surf. Interface Anal.* **2001**, *31*, 954−965.

(11) Sheppard, L. R.; Dittrich, T.; Nowotny, J.; Bak, T. Surface Photovoltage Studies of Nonstoichiometric Rutile Titanium Dioxide. *Appl. Phys. Lett.* **2010**, *96*, 072104.

(12) Nowotny, M. K.; Bogdanoff, P.; Dittrich, T.; Fiechter, S.; Fujishima, A.; Tributsch, H. Observations of p-Type Semiconductivity in Titanium Dioxide at Room Temperature. *Mater. Lett.* **2010**, *64*, 928−930.

(13) Zabel, P.; Dittrich, T.; Funes, M.; Durantini, E. N.; Otero, L. Charge Separation at Pd−Porphyrin/TiO_2 Interfaces. *J. Phys. Chem. C* **2009**, *113*, 21090−21096.

(14) Dittrich, T.; Fiechter, S.; Thomas, A. Surface Photovoltage Spectroscopy of Carbon Nitride Powder. *Appl. Phys. Lett.* **2011**, *99*, 084105.

(15) Beranek, R.; Neumann, B.; Sakthivel, S.; Janczarek, M.; Dittrich, T.; Tributsch, H.; Kisch, H. Exploring the Electronic Structure of Nitrogen-Modified TiO_2 Photocatalysts through Photocurrent and Surface Photovoltage Studies. *Chem. Phys.* **2007**, *339*, 11−19.

(16) Gross, D.; Mora-Sero, I.; Dittrich, T.; Belaidi, A.; Mauser, C.; Houtepen, A. J.; Da Como, E.; Rogach, A. L.; Feldmann, J. Charge Separation in Type II Tunneling Multilayered Structures of CdTe and CdSe Nanocrystals Directly Proven by Surface Photovoltage Spectroscopy. *J. Am. Chem. Soc.* **2010**, *132*, 5981−5983.

(17) Townsend, T. K.; Browning, N. D.; Osterloh, F. E. Overall Photocatalytic Water Splitting with NiO_x−$SrTiO_3$ — A Revised Mechanism. *Energy Environ. Sci.* **2012**, *5*, 9543−9550.

(18) Waller, M.; Townsend, T. K.; Zhao, J.; Sabio, E. M.; Chamousis, R. L.; Browning, N. D.; Osterloh, F. E. Single-Crystal Tungsten Oxide Nanosheets: Photochemical Water Oxidation in the Quantum Confinement Regime. *Chem. Mater.* **2012**, *24*, 698−704.

(19) Osterloh, F. E.; Holmes, M. A.; Chang, L.; Moule, A. J.; Zhao, J. Photochemical Charge Separation in Poly(3-hexylthiophene) (P3HT) Films Observed with Surface Photovoltage Spectroscopy. *J. Phys. Chem. C* **2013**, *117*, 26905−26913.

(20) Dember, H. A Photoelectrical-Motor Energy in Copper-Oxide Crystals. *Phys. Z.* **1931**, *32*, 554−556.

(21) Sarkar, D.; Halas, N. J. Dember Effect in C_{60} Thin-Films. *Solid State Commun.* **1994**, *90*, 261−265.

(22) Maeda, K.; Mallouk, T. E. Comparison of Two- and Three-Layer Restacked Dion−Jacobson Phase Niobate Nanosheets as Catalysts for Photochemical Hydrogen Evolution. *J. Mater. Chem.* **2009**, *19*, 4813−4818.

(23) Compton, O. C.; Osterloh, F. E. Niobate Nanosheets as Catalysts for Photochemical Water Splitting into Hydrogen and Hydrogen Peroxide. *J. Phys. Chem. C* **2009**, *113*, 479−485.

(24) Würfel, P. *Physics of Solar Cells from Principles to New Concepts*; Wiley-VCH: Weinheim, Germany, 2005; p 244.

(25) Treacy, M. M. J.; Rice, S. B.; Jacobson, A. J.; Lewandowski, J. T. Electron Microscopy Study of Delamination in Dispersions of the Perovskite-Related Layered Phases $K[Ca_2Na_{n-3}Nb_nO_{3n+1}]$ − Evidence for Single-Layer Formation. *Chem. Mater.* **1990**, *2*, 279−286.

(26) Virdi, K. S.; Kauffmann, Y.; Ziegler, C.; Ganter, P.; Lotsch, B. V.; Kaplan, W. D.; Blaha, P.; Scheu, C. Electronic Structure of $KCa_2Nb_3O_{10}$ as Envisaged by Density Functional Theory and Valence Electron Energy Loss Spectroscopy. *Phys. Rev. B* **2013**, *87*, 115108.

(27) Duonghong, D.; Gratzel, M. Colloidal TiO_2 Particles as Oxygen Carriers in Photochemical Water Cleavage Systems. *J. Chem. Soc., Chem. Commun.* **1984**, 1597−1599.

(28) Santato, C.; Ulmann, M.; Augustynski, J. Photoelectrochemical Properties of Nanostructured Tungsten Trioxide Films. *J. Phys. Chem. B* **2001**, *105*, 936−940.

(29) Kronik, L.; Ashkenasy, N.; Leibovitch, M.; Fefer, E.; Yoram, S.; Gorer, S.; Hodes, G. Surface States and Photovoltaic Effects in CdSe Quantum Dot Films. *J. Electrochem. Soc.* **1998**, *145*, 1748−1755.

(30) Warren, D. S.; Shapira, Y.; Kisch, H.; McQuillan, A. J. Apparent Semiconductor Type Reversal in Anatase TiO_2 Nanocrystalline Films. *J. Phys. Chem. C* **2007**, *111*, 14286−14289.

(31) Sarkar, S. K.; Hodes, G.; Kronik, L.; Cohen, H. Defect-Dominated Charge Transport in Si-Supported CdSe Nanoparticle Films. *J. Phys. Chem. C* **2008**, *112*, 6564−6570.

(32) Lide, D. R. Electron Work Function of the Elements. In *CRC Handbook of Chemistry and Physics*, 88 (Internet Version 2008) ed.; CRC Press/Taylor and Francis: Boca Raton, FL, 2008.

(33) Aphek, O. B.; Kronik, L.; Leibovitch, M.; Shapira, Y. Quantitative Assessment of the Photosaturation Technique. *Surf. Sci.* **1998**, *409*, 485−500.